

Article

# Comparison of Two Energy Management Strategies Considering Power System Durability for PEMFC-LIB Hybrid Logistics Vehicle

Jianning Liang <sup>1</sup>, Yankun Li <sup>1</sup>, Wenya Jia <sup>2</sup>, Weikang Lin <sup>2</sup> and Tiancai Ma <sup>2,\*</sup> 

<sup>1</sup> CRRC Qingdao Sifang Co. Ltd., Qingdao 266111, China; liangjianning@cqsf.com (J.L.); liyankun@cqsf.com (Y.L.)

<sup>2</sup> School of Automotive Studies, Tongji University, Shanghai 201804, China; jiawenya@tongji.edu.cn (W.J.); weikang.lin@tongji.edu.cn (W.L.)

\* Correspondence: matiancai@tongji.edu.cn; Tel.: +86-21-6958-3814

**Abstract:** For commercial applications, the durability and economy of the fuel cell hybrid system have become obstacles to be overcome, which are not only affected by the performance of core materials and components, but also closely related to the energy management strategy (EMS). This paper takes the 7.9 t fuel cell logistics vehicle as the research object, and designed the EMS from two levels of qualitative and quantitative analysis, which are the composite fuzzy control strategy optimized by genetic algorithm and Pontryagin's minimum principle (PMP) optimized by objective function, respectively. The cost function was constructed and used as the optimization objective to prolong the life of the power system as much as possible on the premise of ensuring the fuel economy. The results indicate that the optimized PMP showed a comprehensive optimal performance, the hydrogen consumption was 3.481 kg/100 km, and the cost was 13.042 \$/h. The major contribution lies in that this paper presents a method to evaluate the effect of different strategies on vehicle performance including fuel economy and durability of the fuel cell and battery. The comparison between the two totally different strategies helps to find a better and effective solution to reduce the lifetime cost.

**Keywords:** proton exchange membrane fuel cell; energy management strategy; fuzzy control; Pontryagin's minimum principle; multi-objective optimization



**Citation:** Liang, J.; Li, Y.; Jia, W.; Lin, W.; Ma, T. Comparison of Two Energy Management Strategies Considering Power System Durability for PEMFC-LIB Hybrid Logistics Vehicle. *Energies* **2021**, *14*, 3262. <https://doi.org/10.3390/en14113262>

Academic Editor: Felix Barreras

Received: 11 May 2021

Accepted: 31 May 2021

Published: 2 June 2021

**Publisher's Note:** MDPI stays neutral with regard to jurisdictional claims in published maps and institutional affiliations.



**Copyright:** © 2021 by the authors. Licensee MDPI, Basel, Switzerland. This article is an open access article distributed under the terms and conditions of the Creative Commons Attribution (CC BY) license (<https://creativecommons.org/licenses/by/4.0/>).

## 1. Introduction

Fuel cells have the advantages of clean and high efficiency, which play important roles in the new round of energy revolution [1]. Proton exchange membrane fuel cells (PEMFCs) are considered as an effective variant to diesel distributed generations that can back up electricity and balance grid power. The hydrogen-fueled cars on the global market have been fed by PEMFCs [2]. However, a standalone fuel cell system cannot meet the demands of the frequent changing load for construction vehicle applications. In addition, the fuel cell system cannot store the regenerative energy. Therefore, there must be at least an auxiliary power source (e.g., a battery) that is everywhere in all forms of transportation and electronics to improve vehicle performance [3].

Although a lot of effort has been made in order to introduce fuel cell vehicles to commercial applications, the main limitations are the cost and durability of the fuel cell system [4]. A good EMS can improve the economy and durability of fuel cell vehicles, thus reducing the lifetime cost of the fuel cell, which has great research and application value [5]. The function of the EMS of hybrid electric vehicles is to control and adjust the powertrain and its components to work normally on the premise of meeting the requirements of vehicle power performance [6]. Nowadays, the research on EMS is divided into rule-based and optimization-based strategies. A review of the control algorithm is represented in Table 1.

The rule-based strategies have strong practicability and high reliability [7–15]. However, most of them are based on the engineering experience, and the results are dependent on the design of the rules. Optimization-based strategies are more effective in optimization. This kind of strategy mainly includes instantaneous and global optimal strategies [16–18]. One of the most classic instantaneous strategies is the equivalent consumption minimization strategy (ECMS). Garcia [17] argued that ECMS was the most appropriate control strategy because it achieved a good balance between hydrogen consumption, efficiency, adaptability, and calculation time. However, the adaptability of ECMS to working conditions is poor, and there are many studies on the adaptive adjustment of equivalent factors. Global optimization strategies mainly include dynamic programming (DP) [19,20] and PMP [21]. Although DP can achieve global optimization, it is not commonly used in engineering practice because of the large amount of calculation, the disaster of dimensionality, and the need to predict the working condition information. Many studies have changed to focus on the PMP strategy. Zheng [21] adopted the PMP to study the fuel cell locomotive, and established the objective function of the minimum hydrogen consumption. The strategies above-mentioned can achieve a satisfactory fuel economy. However, none of them considered fuel cell durability.

**Table 1.** The summary of strategies.

Ref.	Classification	Control Algorithm
[7,10] [8,9] [11] [10,12–14]	Rule-based	Operating mode control Thermostat control State machine control Fuzzy control
[16] [17,18] [19,20] [21]	Optimization-based	Particle swarm optimization ECMS DP PMP

In addition to reducing fuel consumption, how to improve the durability of the fuel cell and battery is very important. Based on frequency separation methods [22,23], strategies have been adopted to avoid drastic power fluctuations of the fuel cell and thus extend its life. However, this kind of strategy ignores fuel economy and might result in high hydrogen consumption. Another approach was to construct a cost function that takes fuel cell durability into account [24]. However, in this research, the weighting factor was hard to decide because of the tradeoff between fuel economy and fuel cell durability. Most control strategies considering degradation do not consider a direct way to include fuel cell and battery degradation.

In light of the above, it is essential to build an effective EMS for improving fuel economy and prolonging the lifetime of the fuel cell. This paper conducted studies to optimize the fuel economy and power system durability to reduce lifetime costs. Several strategies focusing on fuzzy and PMP were compared while considering fuel consumption, fuel cell degradation, and battery capacity decay to minimize lifetime cost under a connected vehicle scenario. The contributions of this study lie in the comparison among these strategies, taking the cost function as the evaluation index. Results showed that the hydrogen consumption was lower, but the cost was higher under the optimized fuzzy strategy. In contrast, under the PMP strategy, the hydrogen consumption was higher but the cost was lower. These findings provide insights into the importance of including component degradation within the energy management system to reduce lifetime cost.

The rest of this paper is organized as follows. First, the model of the powertrain system and vehicle is introduced in Section 2. Then, in Section 3, two energy management strategies are described from aspects of qualitative and quantitative analysis of power system durability separately: the durability of the power system was qualitatively analyzed by the degradation factors of the fuel cell and battery, and quantified by the multi-objective

optimization function. Additionally, the simulation results are presented to contrast and verify the value of the proposed strategy in Section 4. Finally, Section 5 summarizes the conclusions of this paper.

## 2. Powertrain System Modeling

The fuel cell hybrid powertrain system includes fuel cell engine (FCE), DC/DC converter, battery, and motor, as shown in Figure 1. The output voltage of the fuel cell is controlled by adjusting the low voltage end of the DC/DC converter. Table 2 shows the key parameters of the powertrain system and vehicle.

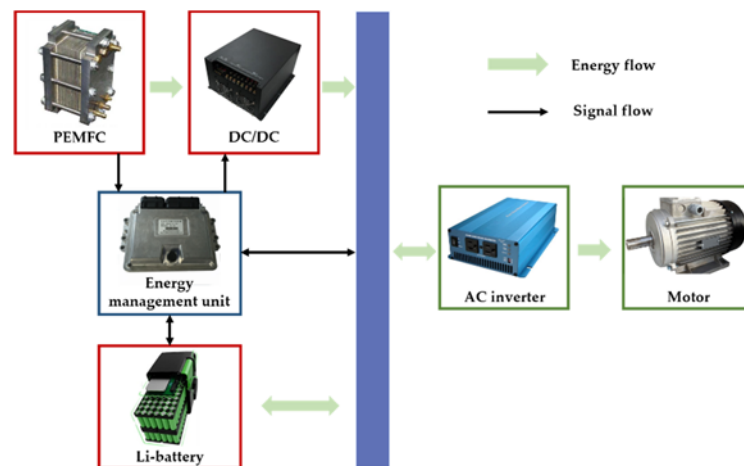


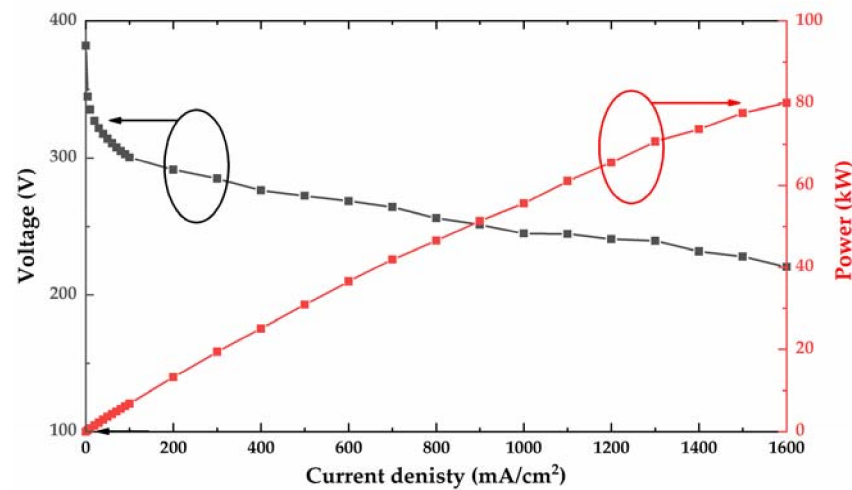
Figure 1. Architecture diagram of the hybrid powertrain system.

Table 2. Main parameters of the powertrain system and vehicle.

Parameter	Parameter	Value
Fuel cell	Cell number	380
	Effective area of cell	227 cm <sup>2</sup>
	Peak power of stack	80 kW
Battery	Cell capacity	26.5 Ah
	Parallel number	3
	Serial number	85
	Peak charge-discharge ratio	4C
Motor	Rated voltage	320 V
	Peak power	4000 kW
	Peak speed	1600 r/min
	Peak torque	80 Nm
	Rated power	800 kW
Vehicle	Rated speed	1024 r/min
	Rated torque	4000 Nm
	Curb Weight	5100 kg
	Full Weight	7900 kg
	Vehicle length	6438 mm
	Rolling resistance coefficient	0.01
	Face area	5.9 m <sup>2</sup>
Drag coefficient	0.7	

### 2.1. Model of PEMFC

When the stack works at the peak power point, which is 80 kW, the power consumption of the auxiliary system is 10 kW. Figure 2 shows the polarization curve of a fuel cell obtained through tests.



**Figure 2.** The polarization curve of the fuel cell stack.

According to the output current of the reaction process, the hydrogen consumption rate of the fuel cell can be calculated as [25]:

$$I_{st} = \frac{nF}{t} \quad (1)$$

$$\dot{m}_{fc} = N_{cell} \cdot \frac{I_{st} M_H}{nF\eta_H} \quad (2)$$

where  $I_{st}$  (A) represents the output current of the fuel cell;  $n$  (which is the number 2) means that for every mole of hydrogen that reacts, two moles of electrons are transferred;  $F$  is the Faraday constant, 96,485 C/mol;  $t$  (s) is the time it takes for each mole of hydrogen to react;  $N_{cell}$  (which is the number 380) represents the number of fuel cell units;  $\dot{m}_{fc}$  (g/s) represents the hydrogen consumption rate of fuel cell;  $N_{cell}$  (g/s) represents the hydrogen consumption rate of fuel cell;  $M_H$  represents the molar mass of hydrogen, 2.016 g/mol; and  $\eta_H$  represents the utilization rate of hydrogen, 97%. The unreacted hydrogen on the anode side, the inert gas, and water infiltrated from the cathode side will first flow through the water separator. The water separator separates most of the liquid water, leaving a small amount of liquid water, inert gas, and hydrogen in the atmosphere through the hydrogen purge valve. From the above process, it can be seen that hydrogen cannot be completely used in the reactor to participate in chemical reactions, and the utilization rate of hydrogen in engineering can reach 97% [26].

Figure 3a shows the relationship between the hydrogen consumption rate and net output power of the fuel cell system, which is obtained by curve fitting as follows:

$$\dot{m}_{fc} = (3 \times 10^{-4}) \times P_{fc}^2 + 0.0097 \times P_{fc} + 0.00374 \quad (3)$$

The fuel cell system efficiency can be calculated based on the hydrogen consumption rate of the fuel cell. It is defined as the ratio of the net output power of the fuel cell system to the low calorific value energy generated by hydrogen. The equation is as follows:

$$\eta_{fc} = \frac{P_{fc}}{\dot{m}_{fc} LHV} \quad (4)$$

where  $\eta_{fc}$  represents the efficiency of the fuel cell system;  $P_{fc}$  (kW) represents the output power of the fuel cell system; and  $LHV$  represents the lower heat value of hydrogen, 119.64 MJ/kg.

Figure 3b shows the relationship between system efficiency and net output power of fuel cell. The reason for the low efficiency of the fuel cell system at the low partial loads is

that the power consumption of the auxiliary system accounts for a large proportion of the power of the stack.

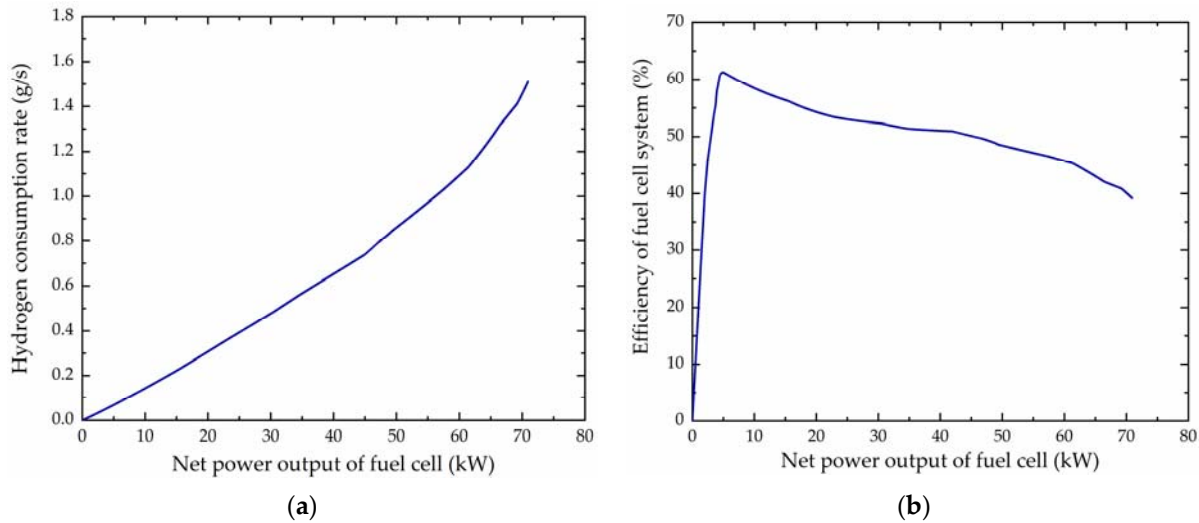


**Figure 3.** Characteristic curves of the fuel cell system. (a) Fuel cell hydrogen consumption rate and net output power curve; (b) Fuel cell system efficiency characteristic curve.

Many studies on the fuel cell degradation model are mainly carried out from the following four kinds of conditions as the starting point: dynamic load change, start-stop, idling, and high-power [27–30]. The discrete equations are shown as follows:

$$D_{fc} = \sum_1^n (d_{start-stop} + d_{load\_change} + d_{low} + d_{high}) \quad (5)$$

$$\text{if } Signal_{engine\_on,n-1} = 0, Signal_{engine\_on,n} = 1, \text{ and } t_{engine\_off} \geq 180 \quad (6)$$

$$d_{start-stop} = 1.96 \times 10^{-3}; \text{ else } d_{start-stop} = 0$$

$$d_{load\_change} = 5.93 \times 10^{-5} \times \frac{|P_{fc,t=n} - P_{fc,t=n-1}|}{(P_{high} - P_{low}) \times 2} \quad (7)$$

$$\text{if } 0 < P_{fc} \leq P_{low}, d_{low} = 1.26 \times 10^{-3} \times \frac{\Delta t}{3600}, \text{ else } d_{low} = 0 \quad (8)$$

$$\text{if } P_{fc} > P_{high}, d_{high} = 1.47 \times 10^{-3} \times \frac{\Delta t}{3600}, \text{ else } d_{high} = 0 \quad (9)$$

where  $D_{fc}$  is the total degradation of fuel cell;  $d_{start-stop}$ ,  $d_{load\_change}$ ,  $d_{low}$ ,  $d_{high}$  are degradation rates under start-stop, dynamic load change, idling, and high-power conditions, respectively;  $Signal_{engine\_on}$  represents the on/off state of the fuel cell engine;  $t_{engine\_off}$  (s) represents the duration time of the off state of fuel cell engine;  $P_{low}$  (kW) and  $P_{high}$  (kW) represent the low-power and high-power threshold of the fuel cell under idling and high-power conditions, respectively. Referring to the recommended voltage operating range of PEMFC [27],  $P_{low}$  is 5.9 kW and  $P_{high}$  is 48.2 kW.

## 2.2. Model of Lithium-Ion Battery

The battery adopts the  $R_{int}$  equivalent circuit model because this kind of model is not only simple and time-efficient, but also has almost the same results as the second-order RC model. Based on the  $R_{int}$  model, the relationships between the battery power, resistance, voltage, and current are shown as:

$$U_b = U_{oc} - I_b R_b \quad (10)$$

$$P_b = U_{oc} \cdot I_b - R_b \cdot I_b^2 \quad (11)$$

$$I_b = \frac{U_{oc} - \sqrt{U_{oc}^2 - 4R_b \cdot P_b}}{2R_b} \quad (12)$$

where  $U_b$  (V) represents the output voltage of lithium-ion battery;  $U_{oc}$  (V) represents the open circuit voltage;  $R_b$  ( $\Omega$ ) is the equivalent internal resistance;  $P_b$  (kW) represents the output power; and  $I_b$  (A) represents the current, when  $I_b > 0$ , the battery is discharged, when  $I_b < 0$ , the battery is charged. The rated voltage of the battery is 320 V.

The ampere hour integration method is used to calculate the state of charge (SOC) of the lithium-ion battery:

$$SOC_t = SOC_0 - \frac{\int_0^t I_b \cdot dt}{3600 \cdot Q} \quad (13)$$

where  $SOC_t$  represents the current state of charge of lithium-ion battery;  $SOC_0$  represents the residual state of charge at the initial time; and  $Q$  (Ah) represents the capacity.

The energy  $E_{bat}$  (kWh) charged/discharged in the battery calculated at the DC bus is as follows [20,31]:

$$E_{bat} = \begin{cases} -\frac{V_{batavg} \cdot \Delta Q_{bat} \cdot \eta_{batdisavg}}{\eta_{DC} \cdot LHV}, & \Delta Q_{bat} > 0, \text{ charging} \\ -\frac{V_{batavg} \cdot \Delta Q_{bat}}{\eta_{DC} \cdot \eta_{batchgavg} \cdot LHV}, & \Delta Q_{bat} \leq 0, \text{ discharging} \end{cases} \quad (14)$$

where  $\eta_{batchgavg}$  and  $\eta_{batdisavg}$  represent the average charge/discharge efficiency of the battery;  $\Delta Q_{bat}$  (Ah) represents the charge/discharge capacity of the battery;  $V_{batavg}$  (V) represents the average voltage of the battery; and  $\eta_{DC}$  represents the efficiency of the DC/DC converter, which was 97% in this paper.

The charge/discharge efficiency of the battery is related to the SOC, charge/discharge internal resistance, and power. The calculation equations are as follows:

$$\eta_{batdisavg} = \frac{1 + \sqrt{1 - \frac{4R_{dis}P_{batdis}}{U_{oc}^2}}}{2} \quad (15)$$

$$\eta_{batchgavg} = \frac{2}{1 + \sqrt{1 - \frac{4R_{chg}P_{batchg}}{U_{oc}^2}}} \quad (16)$$

where  $R_{chg}$  ( $\Omega$ ) and  $R_{dis}$  ( $\Omega$ ) are the internal charge/discharge resistance, respectively; and  $P_{batchg}$  (kW) and  $P_{batdis}$  (kW) are the charge/discharge power, respectively.

The open circuit voltage (OCV) and charge/discharge resistance of battery are not fixed values; they fluctuate with SOC. Charge/discharge cycle experiments were carried out on the selected batteries. Figure 4 shows the obtained OCV and internal resistance of the battery system.

According to the National Renewable Energy Laboratory (NREL), the degradation of the lithium-ion battery is divided into cycle and calendar degradation, and the expression is as follows [32]:

$$Q_{degradation} = Q_{cycle} + Q_{calendar} = (e_0 + e_1 N) + (d_0 + d_1 t^{\frac{1}{2}}) \quad (17)$$

where  $N$  is the number of cycles;  $t$  is the running time;  $e_0$ ,  $e_1$ ,  $d_0$ ,  $d_1$  are expressions related to discharge depth, temperature, and discharge rate. In order to obtain the values of these four parameters, several groups of charge/discharge cycles were carried out in this paper.

By analyzing the experimental results, their values were 0.115, 0.0649, 0.371, and 0.292 under 298.15 K, respectively.

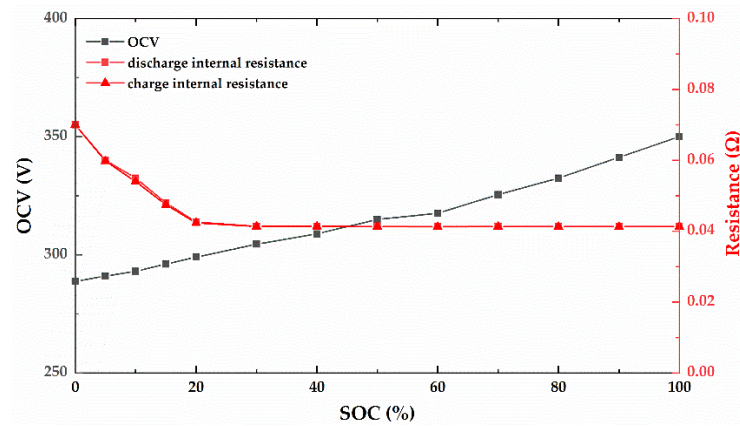


**Figure 4.** Characteristic curves of the lithium-ion battery.

### 2.3. Model of the Vehicle

According to the longitudinal dynamics of the vehicle, the traction force is calculated as follows:

$$F_t = mgf\cos\alpha + \frac{C_D A u^2}{21.15} + mg\sin\alpha + \delta m \frac{du}{dt} \quad (18)$$

where  $F_t$  (N) is the total traction force;  $m$  is the vehicle mass;  $g$  is the acceleration due to gravity, 9.8 N/kg;  $f$  is the rolling resistance coefficient;  $u$  (km/h) is the vehicle velocity;  $\alpha$  ( $^\circ$ ) is the road angle that may be uphill ( $\alpha > 0$ ) or downhill ( $\alpha < 0$ );  $C_D$  is the air drag coefficient; and  $A$  ( $m^2$ ) is the front area. According to the traction force and vehicle speed, the torque on the wheel  $T_W$  (N·m) and the wheel rotation speed  $w_W$  (rad/s) are then calculated by:

$$T_W = r \cdot F_t \quad (19)$$

$$w_W = u/3.6r \quad (20)$$

where  $r$  (m) is the wheel radius. The relationship correlating the fuel cell net power  $P_{fc}$ , battery power  $P_{bat}$ , and the total demanded power  $P_{req}$  (kW) is expressed as follows:

$$P_{req} = P_{fc} \times \eta_{DC} + P_{bat} \quad (21)$$

### 3. Energy Management Strategy Considering Power System Durability

The concept of generalized economy is proposed in this paper. Generalized economy refers to the comprehensive economy that takes durability into consideration. The optimization objectives include two aspects: one is the fuel cell hydrogen consumption, the other is the durability of the power system composed of the fuel cell and battery. The EMS under a qualitative generalized economy adopts the comprehensive strategy of fuzzy control, switch control, and sliding window filtering algorithm, which makes the fuel cell work in the high efficiency area to improve its fuel economy, and slows down the power fluctuation of the fuel cell and the capacity fluctuation of the battery to improve the durability of the power system. The EMS under quantitative generalized economy adopts the PMP, takes the hydrogen consumption of the fuel cell as the economic index, and the power fluctuation of the fuel cell as the durability index. With the solution of the multi-objective optimization function, the optimal power trajectory of the fuel cell is obtained.

### 3.1. Energy Management Strategy under Qualitative Generalized Economy

#### 3.1.1. Composite Fuzzy Control Strategy

The influencing factors of fuel cell durability mainly come from dynamic load change, start-stop, idling, and high-power conditions. In this section, a composite fuzzy control strategy based on switch control and the sliding window filtering algorithm is proposed. The qualitative strategy was formulated to effectively reduce the frequency of the above-mentioned four bad conditions and other operating points that affect the durability of the fuel cell. The switch control strategy can avoid a series of safety problems such as over-charge and over-discharge of the battery. The sliding window filtering algorithm can make the output power of the fuel cell as smooth as possible, which is conducive to improving the durability of the fuel cell.

Figure 5 shows the flow chart of the composite fuzzy energy management strategy.

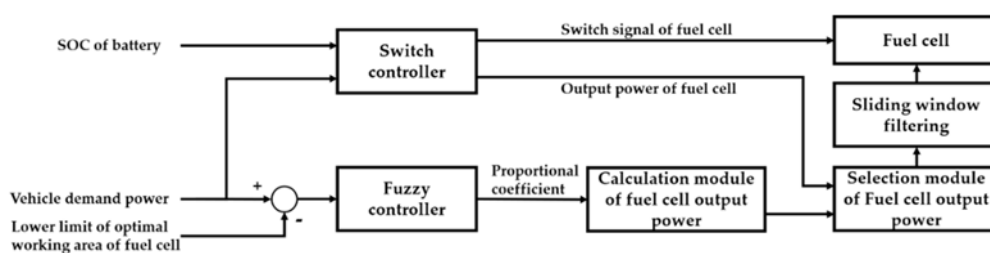


Figure 5. Flow chart of the composite fuzzy energy management strategy.

The design principle of the fuzzy controller is as follows:

- Try to avoid the fuel cell working at idling condition;
- Try to reduce the number of fuel cell start-up and shut-down;
- Make the fuel cell work in a high efficiency area; and
- Keep the SOC of the battery in a reasonable range, which was 40~80% in this paper [33].

The input of the fuzzy controller was set to the SOC of the battery and the difference between the required power of the vehicle and the lower limit of the optimal working area of the fuel cell. The output was proportional to the coefficient  $K$  of the fuel cell output power,  $0 \leq K \leq 1$ . In order to limit the output power of the fuel cell in the optimal working area, the proportional coefficient is expanded proportionally, and the final output power of the fuel cell is  $(8K + 62)$  kW. Table 3 shows the fuzzy rules. The fuzzy subsets are “very small (VS)”, “small (S)”, “middle (M)”, “big (B)”, and “very big (VB)”, respectively. The first column represents the power change. The first row represents the SOC and the values of the intersections represent the values of  $K$ . Figure 6 shows the membership function of each variable.

Table 3. Fuzzy rules.

$K$	SOC				
		VS	S	M	B
$\Delta P$	VS	M	S	VS	VS
S	S	B	M	S	VS
M	M	VB	B	M	S
B	B	VB	B	B	M
VB	VB	VB	VB	B	M

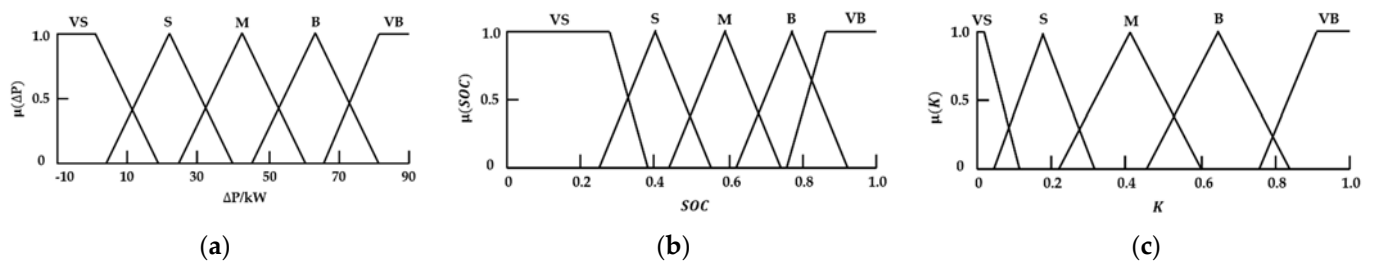


**Figure 6.** Flow chart of the composite fuzzy energy management strategy. (a) Membership function of input power; (b) Membership function of SOC; (c) Membership function of proportional coefficient of fuel cell output power.

Figure 7 shows the flow chart of the switch control strategy (Y means yes, N means No). When the SOC of the battery is higher than the set upper limit, the fuel cell is shut down to make the battery begin to discharge, thus ensuring its safety.

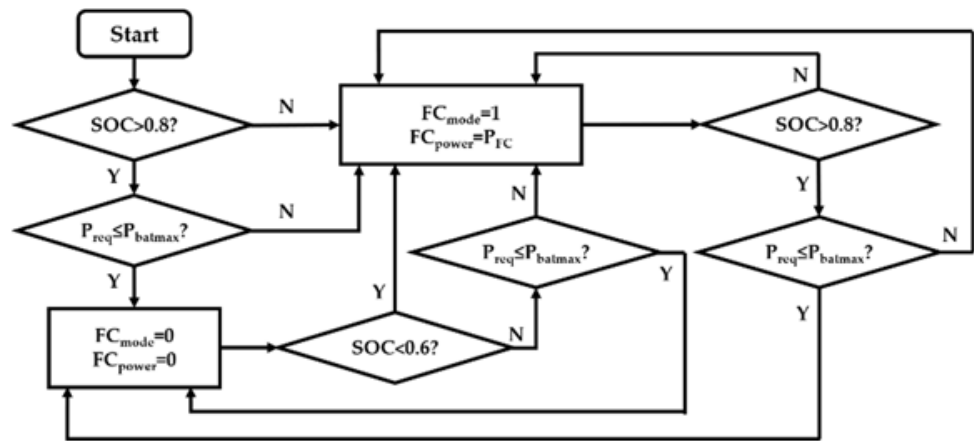


**Figure 7.** Flow chart of the switch control strategy.

In order to further improve the durability of the fuel cell, the sliding window filtering algorithm was adopted to make the output power smoother and the performance damage of the fuel cell caused by the dynamic load change condition was reduced. The expression of fuel cell power output by the sliding window filtering algorithm is as follows:

$$P_{fc} = \frac{1}{N} \times \sum_{k=0}^{N-1} P[T - k] \tag{22}$$

where  $N$  is the number of sampling points contained in the sliding window;  $t$  is the current sampling time;  $k$  is the time axis of the sliding window; and  $P[T - k]$  represents the fuel cell power at the  $k + 1$  sampling point within the sliding window range.

### 3.1.2. Improved Composite Fuzzy Control Strategy Using Genetic Algorithm (GA)

Because the establishment of membership function and fuzzy rules depend on engineering experience, it is difficult to achieve the optimal control effect. Therefore, the genetic algorithm was adopted to optimize the design of the fuzzy controller.

The basic genetic algorithm consists of coding, fitness function, genetic operators (selection, crossover, mutation), and operation parameters. Figure 8 shows the flow chart of the genetic algorithm to solve the optimization problem. First, the population individuals are initialized so that each individual has a potential optimal solution. Then, based on the co-simulation of MATLAB/Simulink and AVL Cruise, the total hydrogen consumption and the degradation of the power system are obtained to calculate the fitness value. When all the individuals in the population have obtained the fitness calculation values, they

enter genetic operations including selection, crossover, and variation. After that, the highly fitted individuals are retained, and the less fitted individuals are eliminated to achieve self-renewal, so that the population evolves toward a higher fitness. So repeatedly, when the number of iterations is reached, the optimal solution among all the individuals is obtained. At the same time, the optimal membership function has been achieved.

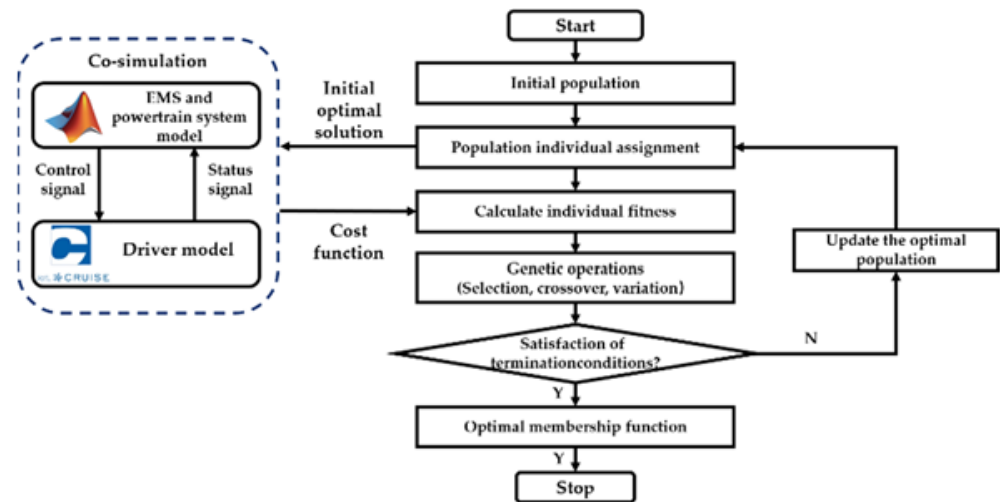


Figure 8. Genetic algorithm optimization process.

Referring to [20,34], in order to consider both fuel economy and power system durability, the cost function related to fuel cell degradation, battery decay, and hydrogen consumption is introduced.

$$\text{cost} = \frac{\left( \frac{D_{fc}}{10} \times C_{fc} \times P_{fcmax} + \frac{D_{bat}}{20} \times C_{bat} \times C_{batmax} + \frac{M}{1000} \times C_{H2} + E_{bat} \times C_{ele} \right)}{x} \quad (23)$$

where cost (\$/h) is the total cost per hour;  $D_{fc}$  (%) and  $D_{bat}$  (%) are the degradation of fuel cell and battery, respectively;  $C_{fc}$  (\$/kW) and  $C_{bat}$  (\$/kWh) refer to the unit cost of the fuel cell and lithium-ion battery;  $P_{fcmax}$  (kW) is the peak power of the fuel cell system;  $C_{batmax}$  (kWh) is the total energy of the battery;  $M$  (g) is the total hydrogen consumption;  $C_{H2}$  (\$/kg) is the unit price of hydrogen;  $C_{ele}$  (\$/kWh) is the unit price of the electric charge/discharge;  $E_{bat}$  (kWh) is the amount of charge/discharge in the working condition; and  $x$  (h) is the operation time. According to the investigation report of the U.S. Department of Energy (DOE), NREL and strategic analysis Inc.,  $C_{fc}$  is taken as \$150/kW,  $C_{bat}$  is taken as \$200/kWh, and  $C_{H2}$  is taken as \$5/kg [35–37]. Based on the report of AMPLY,  $C_{ele}$  is taken as \$0.3/kWh [38].

Due to the long coding length, and taking the reliability and computing speed of the genetic algorithm into account, the population size and the algebra were taken as 20 and 10, respectively. The crossover probability and the mutation probability were taken as 0.7, respectively.

### 3.2. Energy Management Strategy under Quantitative Generalized Economy

Based on PMP, an EMS considering both fuel economy and power system durability was proposed. The hydrogen consumption and output power change rate of the fuel cell were integrated into the multi-objective function to be optimized, and the global optimization was achieved.

### 3.2.1. Optimization Problem Formation and Basic Optimization Goal Setting

According to Equation (13), the value of the SOC change rate of battery  $\dot{SOC}$  ( $s^{-1}$ ) is calculated as follows:

$$\dot{SOC}(t) = -\frac{I_b(t)}{Q} = -\frac{U_{oc}(t) - \sqrt{U_{oc}(t)^2 - 4R_b P_b(t)}}{2R_b Q} \quad (24)$$

Based on PMP,  $P_{fc}$  is defined as the control variable of the system; SOC is the state variable;  $\lambda$  is the co-state;  $t_0$  (s) is the start time; and  $t_f$  (s) is the end time. The control problem is to find the optimal control variable  $P_{fc}^*$  enabling the controlled system shown in Equation (26) to transfer from the given initial state to the terminal state, and to minimize the performance function, as defined in Equation (25). The performance function with the hydrogen consumption as the optimization objective is:

$$\int_{t_0}^{t_f} \dot{m}_{fc}(P_{fc}(t)) dt \quad (25)$$

The state equation is as follows:

$$\dot{SOC}(t) = f(SOC(t), P_{fc}(t), t) \quad (26)$$

The Hamiltonian equation is as follows:

$$H(SOC(t), P_{fc}(t), \lambda(t), t) = \dot{m}_{fc}(P_{fc}(t)) - \lambda(t) \cdot \frac{I_b(P_{fc}(t), SOC(t), t)}{Q} \quad (27)$$

The co-state variables and state variables need to satisfy the regular equations:

$$\dot{\lambda} = -\frac{\partial H}{\partial SOC} = \frac{\lambda \cdot \eta_{bat}}{Q} \left( \frac{\partial I_b}{\partial U_{oc}} \frac{\partial U_{oc}}{\partial SOC} + \frac{\partial I_b}{\partial R_b} \frac{\partial R_b}{\partial SOC} \right) \quad (28)$$

$$SOC^*(t) = \frac{\partial H(SOC^*(t), P_{fc}^*(t), \lambda^*(t), t)}{\partial \lambda} = f(SOC^*(t), P_{fc}^*(t), t) \quad (29)$$

where  $\eta_{bat}$  represents the charge/discharge efficiency of battery; and \* represents the optimal trajectory.

The battery SOC changes in the range of [40%, 80%]. According to Figure 4, in this region of SOC, the relationship between OCV and internal resistance with SOC is as follows:

$$R_b = \text{constant} \quad (30)$$

$$U_{oc} = (4 \times 10^{-5}) \cdot SOC^3 - 0.0036 \cdot SOC^2 + 0.5982 \cdot SOC + 288.15 \quad (31)$$

Equation (28) can be simplified into:

$$\dot{\lambda} = -\frac{\lambda \eta_{bat} I_b(-0.0072x + 0.5982x)}{Q \sqrt{U_{oc}^2 - 4P_b R_b}} \quad (32)$$

The state variable shall satisfy the boundary conditions:

$$SOC(t_0) = SOC(t_f) = SOC_{ref} \quad (33)$$

where  $SOC_{ref}$  represents the reference value of the SOC of the battery, which is generally taken to be 60%.

PMP provides a set of necessary conditions that must be satisfied by the optimal control trajectory. The conditions are as follows:

$$P_{fc}(t) \in \left[ \begin{array}{l} \max \left( P_{fc\text{low}}, \frac{(P_{req}(t) - P_{bathigh}(t))}{\eta_{DC}} \right) \\ \min \left( P_{fc\text{high}}, \frac{(P_{req}(t) - P_{batlow}(t))}{\eta_{DC}} \right) \end{array} \right], \quad (34)$$

$$\left\{ \begin{array}{l} SOC_{low} < SOC < SOC_{high} \\ |SOC(t_f) - SOC_{ref}| < \Delta SOC \\ P_{batlow} < P_b < P_{bathigh} \end{array} \right. \quad (35)$$

where  $P_{fc\text{low}}$  (kW),  $P_{fc\text{high}}$  (kW) represent the low and high limit power of fuel cell respectively;  $P_{batlow}$  (kW),  $P_{bathigh}$  (kW) represent the low and high limit power of the battery, respectively;  $SOC_{low}$ ,  $SOC_{high}$  represent the low and high limit state of charge of the battery, respectively; and  $\Delta SOC$  represents the allowable margin of error, which is generally taken to be 0.0001 [19].

According to PMP, the optimal fuel cell system output power  $P_{fc}^*$  at each time satisfies the following equation:

$$P_{fc}^* = \operatorname{argmin} H \quad (36)$$

PMP states that the optimal solution should minimize the Hamiltonian as follow:

$$H(SOC^*(t), P_{fc}^*(t), \lambda^*(t)) = H(SOC^*(t), P_{fc}(t), \lambda^*(t)) \quad (37)$$

The Hamiltonian can be solved at each instant. When an initial value of  $\lambda$  is set, the co-state variable  $\lambda$  can be calculated based on Equation (32). Under the extreme conditions, the optimal trajectory of the fuel cell output power can be obtained when the Hamiltonian obtains the minimum value. At the same time, the optimal control variable is obtained. By substituting the optimal control variable into the state equation, the change rate of the battery SOC can be obtained, and the current SOC can be calculated according to the ampere-hour integral method. According to the analysis, under the fixed  $\lambda$ , the final SOC value at the end of the working condition is also fixed. There is a monotonic relationship between the co-state variable and the final SOC value [39,40]. Therefore, the initial value of the co-state variable can be obtained by dichotomy.

### 3.2.2. Improved Optimization Objective Based on Fuel Cell Power Change Rate

In the fuel cell hybrid system, the durability of the fuel cell is given priority because of the relatively high cost compared with the lithium-ion battery. In the above section, the performance function, which was established based on PMP, only considers the hydrogen consumption without considering the durability of the fuel cell. In order to optimize the EMS, the fuel cell power change rate was added into the performance function. The improved performance function is as follows:

$$J = \sum_{k=0}^{N-1} (C_{sys,k} + kW_{total,k}) \quad (38)$$

where  $C_{sys,k}$  (g) represents the hydrogen consumption;  $W_{total,k}$  (kW) represents the fuel cell power fluctuation;  $k$  represents the weight factor of the power fluctuation of the fuel cell.

The improved Hamiltonian function is:

$$H = C_{sys,k} + kW_{total,k} + \lambda \dot{SOC} \quad (39)$$

Under the CWTVC condition, the initial  $\lambda$  of the battery SOC is  $-1910$  when the fluctuation of the battery SOC is 0 by the dichotomy method.

After the optimal  $\lambda$  is obtained by using dichotomy, a model based on the optimal  $\lambda$  is built in Simulink to realize online simulation. The simulation step is 0.1 s, and the online PMP strategy can be realized by co-simulation with the vehicle model.

#### 4. Results and Discussion

##### 4.1. Results of Energy Management Strategy under Qualitative Generalized Economy

###### 4.1.1. Verification of Optimization Effect of Composite Fuzzy Control Strategy

In order to prove the optimization effect of the composite fuzzy control strategy, a comparison between the switching control strategy, sliding window filtering strategy, and composite fuzzy strategy was carried out, as shown in Table 4. The start value of SOC was 60% in all strategies. There are some conclusions about the composite fuzzy strategy:

1. Compared with the switch control strategy, the hydrogen consumption per 100 km was increased by 5.250%, while the cost was reduced by 5.825%. This is because in the switching control strategy, the fuel cell is in a constant power operating point for a long time, and the frequency of the dynamic load change condition is almost zero. In order to fill the power demand of the bus, the battery is in a state of deep charge/discharge for a long time, which causes great damage to the battery. The composite fuzzy strategy greatly alleviates the fluctuation of the battery and is beneficial to the extension of the battery life; and
2. Compared with the sliding window filtering strategy, the hydrogen consumption per 100 km was significantly reduced, and the cost was decreased by 0.618%. At the same time, the total degradation rate of the fuel cell was reduced.

**Table 4.** Comparison of economy and durability under different strategies.

Strategy	SOC End Value/%	Hydrogen Consumption/(kg/100 km)	Cost/(\$/h)
1. Switch control	57.489	3.257	14.352
2. Sliding window filtering	59.314	3.561	13.600
3. Composite fuzzy strategy	58.929	3.428	13.516
3 vs. 1	-	+5.250%	-5.825%
3 vs. 2	-	-3.735%	-0.618%

###### 4.1.2. Verification of Effect of the Improved Composite Fuzzy Control Strategy by Using Genetic Algorithm

Figure 9 shows the simulation results of the composite fuzzy strategy before and after the improvement of the genetic algorithm.

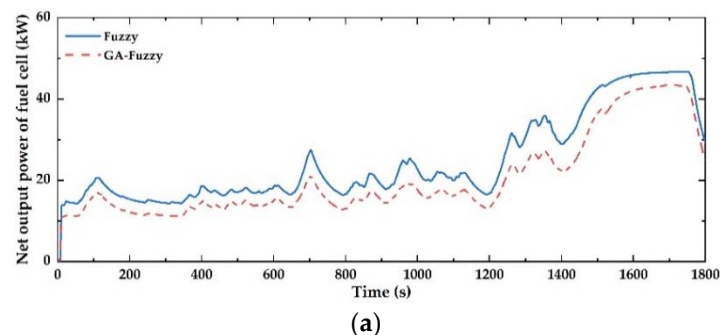


**Figure 9.** Cont.

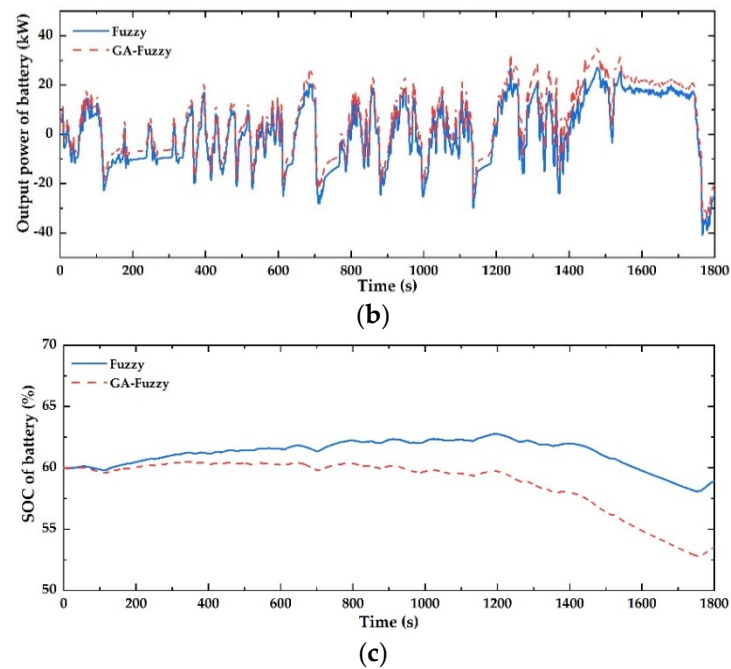


**Figure 9.** Comparison of the fuzzy and GA-fuzzy simulation results. (a) Fuel cell net output power; (b) Battery output power; (c) Battery SOC fluctuation.

Table 5 shows the comparison of the fuel economy and power system durability of the composite fuzzy control strategy before and after improvement.

**Table 5.** Comparison of the economy and durability of the composite fuzzy control strategy before and after improvement.

Strategy	SOC End Value/%	Hydrogen Consumption/ (kg/100 km)	Cost/(\$/h)
1. Composite fuzzy	58.929	3.428	13.516
2. GA-Fuzzy	57.763	3.317	13.339
2 vs. 1	-	-3.238%	-1.310%

It can be seen that compared with before, the hydrogen consumption per 100 km was reduced by 3.238%, and the cost was reduced by 1.310%. At the same time, the total degradation of the fuel cell was reduced. This shows that after using the GA, the fuel economy and fuel cell durability were improved.

#### 4.2. Results of Energy Management Strategy under Quantitative Generalized Economy

According to the influence factors of the four conditions on the fuel cell degradation, the dynamic load change condition had the greatest influence. It can be seen that the selection of the weight factor  $k$  based on the improved PMP is particularly important. The comparison of the fuel cell output power between the improved PMP (P-PMP,  $k = 1 \times 10^{-4}$ ) and the PMP (PMP,  $k = 0$ ) is shown in Figure 10. It can be seen that the power fluctuation of the fuel cell was weakened under P-PMP, so the degradation of the fuel cell because of the dynamic load change condition was reduced. The durability of the fuel cell was improved.

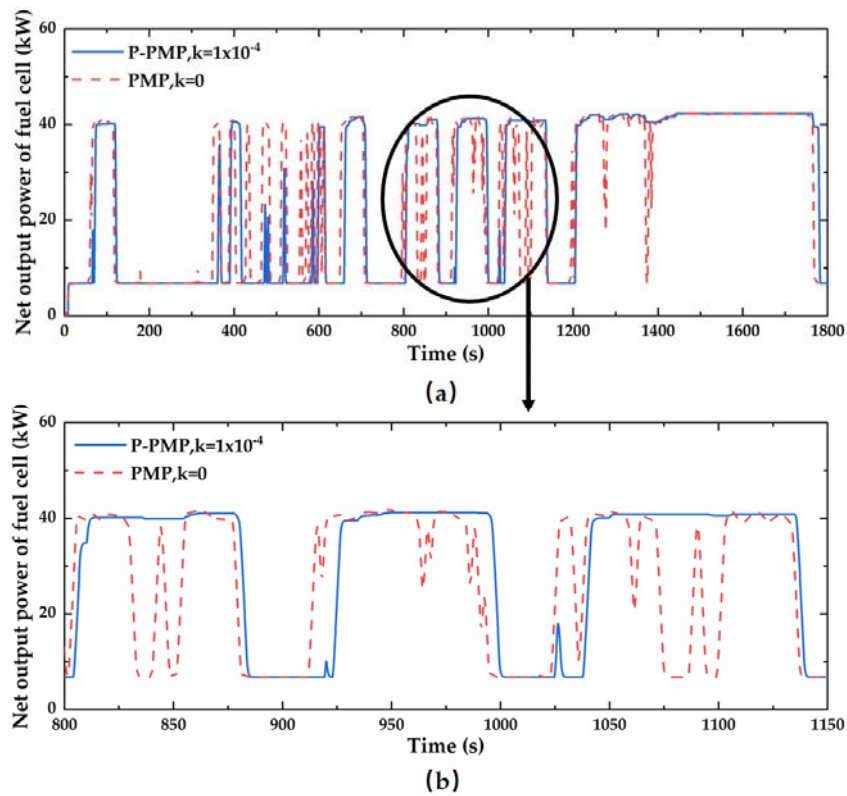


Figure 10. Comparison of the net output power of fuel cell under PMP and P-PMP. (a) Comparison of net output power of fuel cell; (b) Partial enlarged drawing.

Figure 11 shows the results of the fuel economy and power system durability between PMP ( $k = 0$ ) and the P-PMP when the  $k$  value is  $8 \times 10^{-5}$ ,  $1 \times 10^{-4}$ , and  $1.2 \times 10^{-4}$ , respectively.

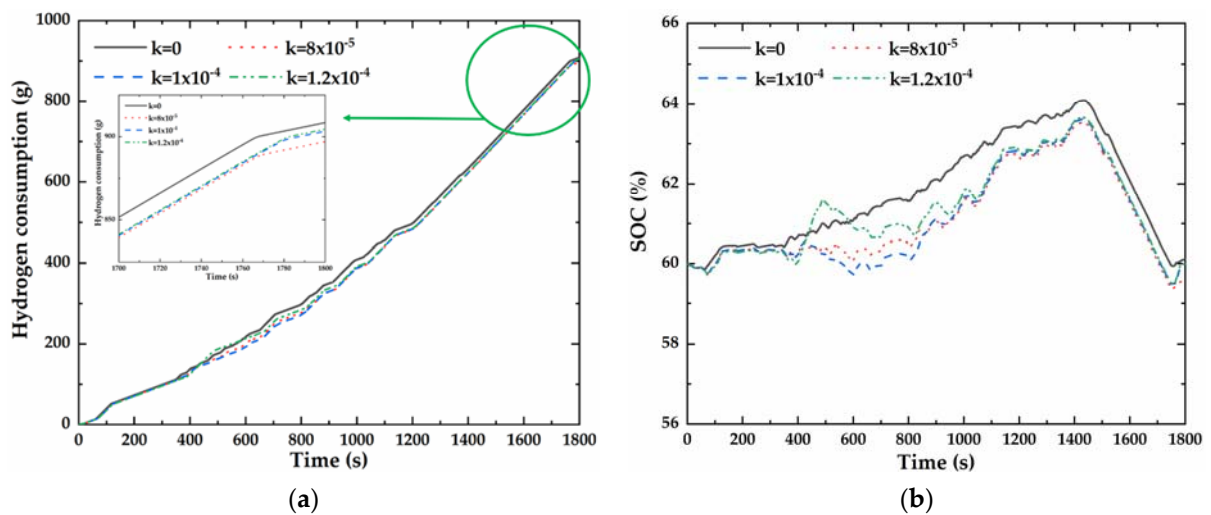
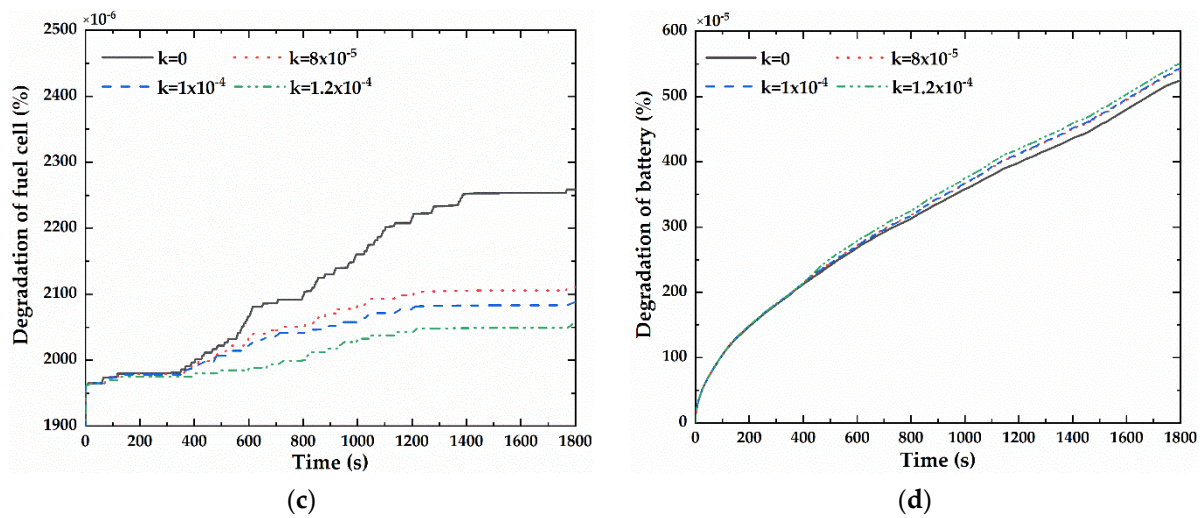


Figure 11. Cont.

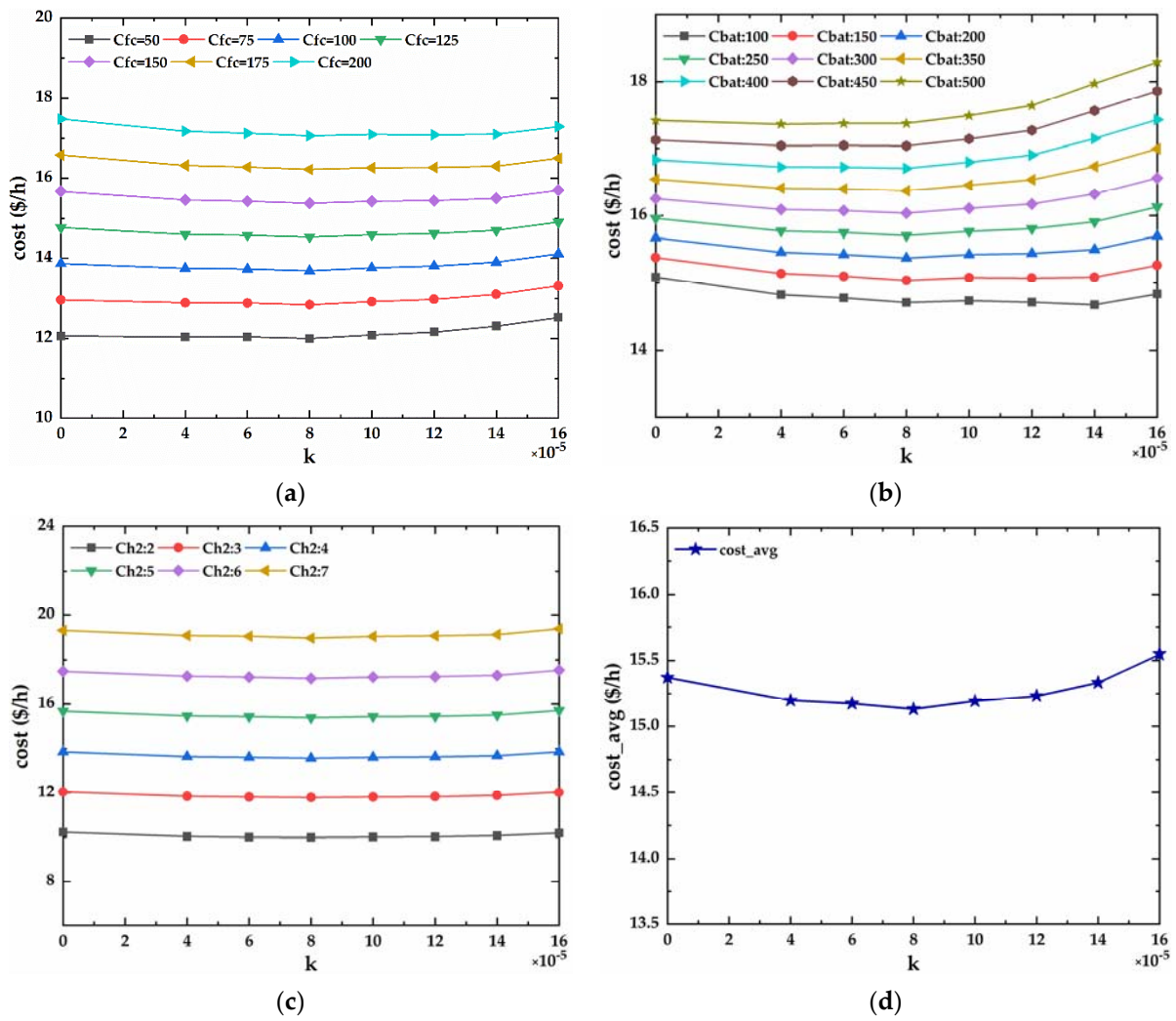


**Figure 11.** Comparison of fuel economy and power system durability under PMP and P-PMP. (a) Total hydrogen consumption; (b) SOC fluctuation; (c) Fuel cell degradation; (d) Battery degradation.

Compared with the results before improvement, the P-PMP had the following characteristics:

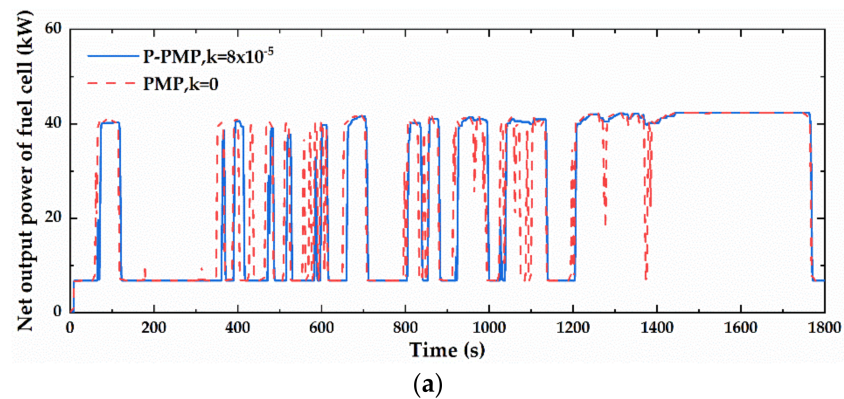
- The fuel economy was improved under the three  $k$  values;
- The difference between the peak and valley of SOC under three  $k$  values decreased, but the degradation degree of the battery increased, which indicates that the small fluctuation of SOC during working condition is relatively larger than that before improvement, which is not conducive to the maintenance of battery life;
- The degradation of fuel cell under three  $k$  values was lower than that before improvement, which indicates that the improvement strategy has a significant effect on improving the fuel cell durability; and
- It can be seen from Figure 11c,d that the larger the value of  $k$ , the less impact the dynamic load change condition has on the degradation of the fuel cell, which is more conducive to improving the fuel cell durability, despite the battery durability being relatively poor. This reflects that different values of  $k$  have different effects on the durability of the fuel cell and battery, so the concept of total cost function is helpful to further select the best value of  $k$ , which makes the fuel economy and power system durability relatively better.

Figure 12 shows the relationship between the cost function and value of  $k$  under different unit price gradients. When  $k$  is taken as  $8 \times 10^{-5}$ , the cost function can keep the lowest for a long time in a large range of power system unit price, which means that the economy and durability of the vehicle reach the comprehensive optimum.



**Figure 12.** Comparison of the curve of cost function with  $k$  value under different unit price. (a)  $C_{fc} = 50:25:200$ ,  $C_{bat} = 200$ ,  $C_{H2} = 5$ ; (b)  $C_{fc} = 150$ ,  $C_{bat} = 100:50:500$ ,  $C_{H2} = 5$ ; (c)  $C_{fc} = 150$ ,  $C_{bat} = 200$ ,  $C_{H2} = 2:1:7$ ; (d) Average value.

Comparing the P-PMP strategy when  $k$  is  $8 \times 10^{-5}$  with the PMP strategy only considering fuel economy, the simulation results under CWTVC condition are shown in Figure 13.



**Figure 13.** Cont.

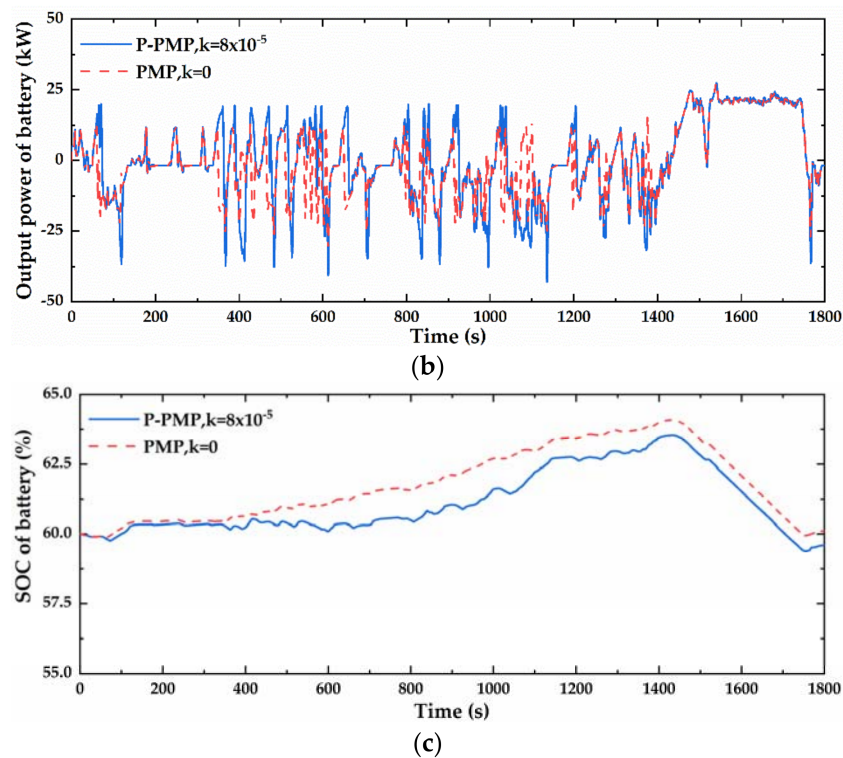


**Figure 13.** Comparison of the simulation results under P-PMP and PMP strategies. (a) Net output power of fuel cell; (b) Output power of battery; (c) SOC fluctuation of battery.

Under the P-PMP strategy, the hydrogen consumption was 3.481 kg/100 km, while the value was 3.540 kg/100 km under the PMP strategy. Combined with the other simulation results, it can be seen that P-PMP strategy has the following characteristics compared with the PMP strategy:

- The output power of the fuel cell was smoother, and the influence of the dynamic load change condition on fuel cell degradation was reduced;
- The absolute value of the SOC fluctuation of the battery  $|\Sigma\Delta SOC|$  was smaller;
- The total hydrogen consumption was smaller and the fuel economy was better; and
- The total degradation of the fuel cell was smaller. Although the total degradation rate of the battery was slightly larger, the lifetime cost was lower.

#### 4.3. Comparison of Fuel Economy and Power System Durability under Different Strategies

This section compares the economic index, durability index, and lifetime cost under different strategies. Among them, the economic index is represented by hydrogen consumption per 100 km, the durability index is represented by fuel cell and battery degradation, and the lifetime cost is represented by cost function.

Table 6 shows the comparison of the simulation results under the CWTVC condition. Figure 14 shows the working efficiency distribution of the fuel cell. The blue bar chart shows the frequency of the power corresponding to the bar in the whole working condition. In this way, the efficiency distribution of the fuel cell can be easily seen.

According to the simulation results, we can get the following results:

- The hydrogen consumption per 100 km was the lowest under the P-PMP strategy, which was 3.481 kg/100 km. At the same time, the lifetime cost was also the lowest among all strategies, which was 13.042 \$/h;
- The total fuel cell degradation was low under the switch control strategy, because the fuel cell has been working at some fixed power point, so the frequency of the dynamic load change condition was very small. According to the power distribution diagram of the fuel cell, the frequency of fuel cell working in the high efficiency

area was higher under this strategy, and the heat loss of hydrogen in the process of energy conversion was less. Therefore, the hydrogen consumption per 100 km was relatively low. However, it also led to frequent fluctuations and a high degradation rate in the batteries. It ended with a relatively high lifetime cost compared with the other strategies;

- Under the sliding window filtering strategy, the total degradation of the fuel cell and battery were at the middle level. At the same time, the hydrogen consumption was higher. According to the efficiency distribution of the fuel cell, the working point of the fuel cell was more scattered under this strategy. Compared with the other strategies, the fuel cell worked more frequently at low efficiency, so the energy loss of hydrogen during energy conversion was larger;
- Compared with the GA-fuzzy strategy, the total fuel cell degradation was increased by 5.79% in the P-PMP strategy. In addition, the battery degradation decreased, the hydrogen consumption per 100 km was smaller, and the final cost was 2.23% smaller; and
- Compared with the PMP strategy, the frequency of the fuel cell working in the high efficiency zone was higher and the hydrogen consumption per 100 km was lower under the P-PMP strategy. In addition, the total degradation of the fuel cell was greatly improved, and the cost was also 1.14% lower.

**Table 6.** Comparison of fuel economy and power system durability under different strategies.

Strategy	Degradation of Fuel Cell/ % × 10 <sup>-5</sup>		Degradation of Battery/ % × 10 <sup>-5</sup>		Hydrogen Consumption/ (kg/100 km)	Cost/(\$/h)
	Dynamic Load Change	Total	Cycle	Total		
1. Switch control	0.33	196.65	111.49	4319.55	3.257	14.352
2. Sliding window filtering	4.45	213.28	63.45	4271.51	3.561	13.600
3. Composite fuzzy	2.64	206.90	80.19	4288.25	3.428	13.516
4. GA-fuzzy	2.28	198.60	81.47	4289.53	3.317	13.339
5. PMP	26.78	223.26	46.33	4254.39	3.540	13.192
6. P-PMP	13.63	210.10	53.15	4261.21	3.481	13.042
6 vs. 1	-	+6.84%	-	-1.35%	+6.88%	-7.73%
6 vs. 2	-	-1.49%	-	-0.24%	-2.25%	-2.63%
6 vs. 3	-	+1.55%	-	-0.63%	+1.55%	-2.03%
6 vs. 4	-	+5.79%	-	-0.66%	+4.94%	-2.23%
6 vs. 5	-	-5.89%	-	+0.16%	-1.67%	-1.14%

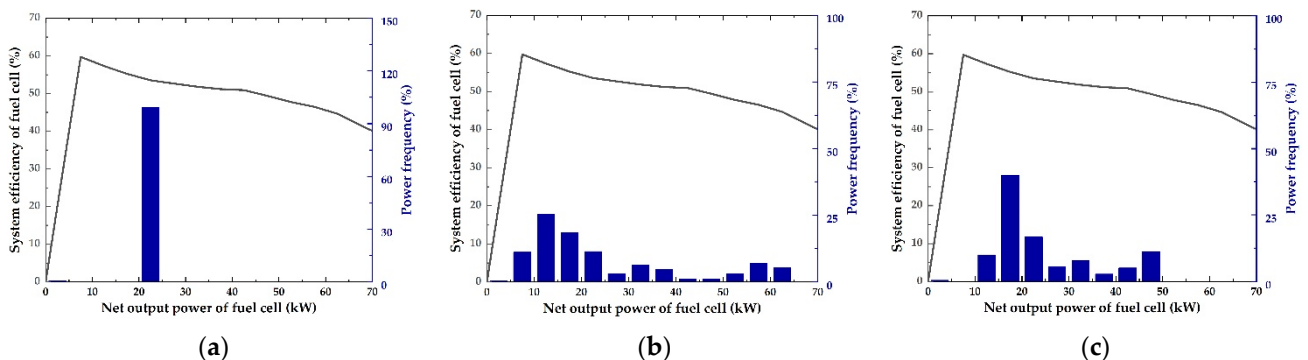


**Figure 14.** Cont.

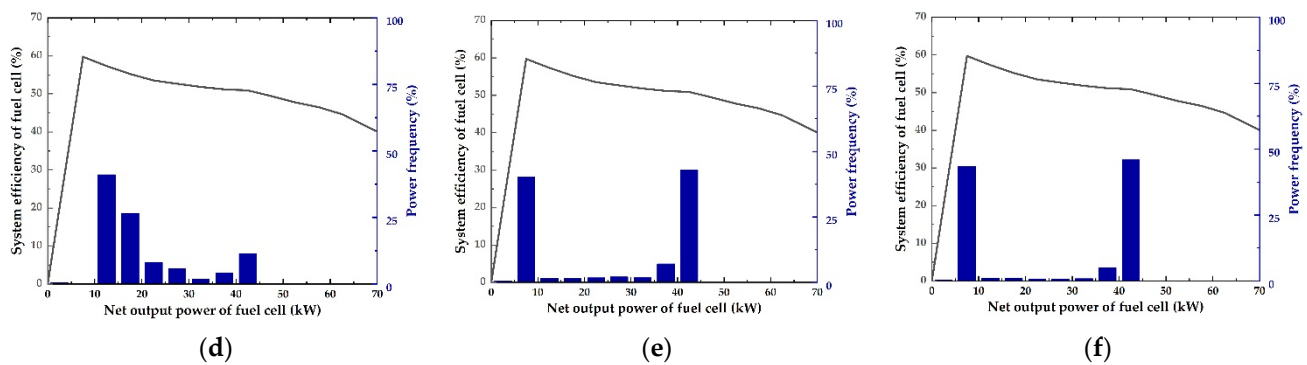


**Figure 14.** The efficiency distribution of the fuel cell with different strategies under CWTVC conditions. (a) Switch control strategy; (b) Sliding window filtering strategy; (c) Composite fuzzy strategy; (d) GA-fuzzy strategy; (e) PMP strategy; (f) P-PMP strategy.

## 5. Conclusions

This paper mainly studied the EMS under a generalized economy, which considers both the fuel economy and the durability of power system. From two levels of qualitative and quantitative analysis, the comprehensive optimization control of multi-objectives in different scales was studied, aiming at the fuel economy and power system durability. First, a method of optimized fuzzy rules by adopting GA was proposed to solve the problem that traditional fuzzy control depends on engineering experience. Under the GA-fuzzy strategy, both hydrogen consumption and cost were reduced. Second, based on the PMP strategy, fuel economy and fuel cell durability were fitted into the objective function. Compared with the strategy considering only fuel economy, the hydrogen consumption, fuel cell durability, and lifetime cost under the P-PMP strategy were all reduced. Third, taking hydrogen consumption, fuel cell degradation, battery decay, and energy consumption all into account, the lifetime cost function was proposed as the ultimate evaluation index. Finally, the simulation results showed that the P-PMP shows comprehensive optimal performance. The hydrogen consumption per 100 km was 3.481 kg/100 km under the CWTVC condition, and the unit time cost was 13.042 \$/h. This indicates that the P-PMP strategy is an effective solution to optimize fuel economy and power system durability.

In future research, the following work will be further carried out: (1) The conclusion might only be valid for the vehicle configuration and drive cycle with the current market costs, so a research method suitable for dynamic market cost is worth exploring; and (2) hardware-in-the-loop and vehicle experiments can be carried out to further verify the effectiveness of the strategies.

**Author Contributions:** Conceptualization, J.L., Y.L. and T.M.; Methodology, J.L.; Software, Y.L.; Validation, J.L. and T.M.; Formal analysis, W.J. and W.L.; Investigation, Y.L.; Resources, T.M. and J.L.; Data curation, W.J. and W.L.; Writing—original draft, J.L., W.J. and Y.L.; Writing—review & editing, J.L., Y.L. and W.L.; Visualization, W.J. and W.L.; Supervision, T.M. and J.L.; Project administration, T.M. and J.L.; Funding acquisition, T.M. and J.L. All authors have read and agreed to the published version of the manuscript.

**Funding:** This research was funded by CRRC Qingdao Sifang Co., Ltd. (Next generation fuel cell air conditioning power supply system for Metro).

**Data Availability Statement:** Not applicable.

**Conflicts of Interest:** The authors declare no conflict of interest.

## Nomenclature

Acronyms

EMS	Energy management strategy
PMP	Pontryagin's minimum principle
PEMFCs	Proton exchange membrane fuel cells

ECMS	Equivalent consumption minimization strategy
DP	Dynamic programming
FCE	Fuel cell engine
OCV	Open circuit voltage
NREL	National Renewable Energy Laboratory
SOC	State of charge
GA	Genetic algorithm
P-PMP	Improved Pontryagin's minimum principle
Symbols	
$I_{st}$	Output current of fuel cell
$n$	Moles of electrons
$F$	Faraday constant
$\dot{m}_{fc}$	Hydrogen consumption rate of fuel cell
$N_{cell}$	Number of fuel cell units
$M_H$	Molar mass of hydrogen
$\eta_H$	Utilization rate of hydrogen
$P_{fc}$	Output power of fuel cell system
$LHV$	Lower heat value of hydrogen
$\eta_{fc}$	Efficiency of fuel cell system
$D_{fc}$	Total degradation of fuel cell
$d_{start-stop}$	Degradation rate under start-stop condition
$d_{load\_change}$	Degradation rate under dynamic load change condition
$d_{low}$	Degradation rates under idling condition
$d_{high}$	Degradation rates under high-power condition
$P_{low}$	Low-power threshold of fuel cell under idling condition
$P_{high}$	High-power threshold of fuel cell under high-power condition
$Signal_{engine\_on}$	On/off state of the fuel cell engine
$t_{engine\_off}$	Duration time of the off state of fuel cell engine
$U_b$	Output voltage of battery
$U_{oc}$	Open circuit voltage of battery
$P_b$	Output power of battery
$R_b$	Equivalent internal resistance of battery
$I_b$	Current of battery
$SOC_t$	Current state of charge of battery
$SOC_0$	Residual state of charge of battery at the initial time
$Q$	Capacity of battery
$E_{bat}$	Charged/discharged in the battery calculated at the dc bus
$\Delta Q_{bat}$	Charge/discharge capacity of battery
$V_{batavg}$	Average voltage of battery
$\eta_{DC}$	Efficiency of dc/dc converter
$R_{chg}$	Internal charge resistance of battery
$R_{dis}$	Internal discharge resistance of battery
$P_{batchg}$	Charge power of battery
$P_{batdis}$	Discharge power of battery
$\eta_{batchgavg}$	Average charge efficiency of battery
$\eta_{batdisavg}$	Average discharge efficiency of battery
$Q_{degradation}$	Total degradation of battery
$Q_{cycle}$	Cycle degradation of battery
$Q_{calendar}$	Calendar degradation of battery
$F_t$	Total traction force
$m$	Vehicle mass
$g$	Acceleration due to gravity
$f$	Rolling resistance coefficient
$u$	Vehicle velocity
$A$	Front area

$\alpha$	Road angle
$C_D$	Air drag coefficient
$T_W$	Torque on the wheel
$w_W$	Wheel rotation speed
$P_{req}$	Total demanded power
$D_{bat}$	Degradation of battery
$C_{fc}$	Unit cost of fuel cell
$C_{bat}$	Unit cost of battery
$P_{fcmax}$	Peak power of the fuel cell system
$C_{batmax}$	Total energy of the battery
$M$	Total hydrogen consumption
$C_{H2}$	Unit price of hydrogen
$C_{ele}$	Unit price of the electric charge/discharge
$\dot{SOC}$	SOC change rate of battery
$\lambda$	Co-state variable
$t_0$	Start time
$t_f$	End time
$\eta_{bat}$	Charge/discharge efficiency of battery
$SOC_{ref}$	Reference value of the SOC of battery
$P_{fclow}$	Low limit power of fuel cell
$P_{fchigh}$	High limit power of fuel cell
$P_{batlow}$	Low limit power of battery
$P_{bathigh}$	High limit power of battery
$SOC_{low}$	Low limit state of charge of battery
$SOC_{high}$	High limit state of charge of battery
$\Delta SOC$	Allowable margin of error of the end SOC of battery
$C_{sys,k}$	Hydrogen consumption
$W_{total,k}$	Fuel cell power fluctuation
$k$	Weight factor of the power fluctuation of fuel cell
<b>Subscripts</b>	
$st$	Stable
$fc$	Fuel cell
$H$	Hydrogen
$cell$	Fuel cell units
$start-stop$	Start-stop condition
$load-change$	Dynamic load change condition
$low$	Idling condition
$high$	High-power condition
$engine\_on$	On state of fuel cell engine
$engine\_off$	Off state of fuel cell engine
$b$	Battery
$oc$	Open circuit
$t$	Current state
$0$	Initial state
$bat$	Battery
$DC$	DC/DC converter
$chg$	Charge
$dis$	Discharge
$avg$	Average
$D$	Drag
$w$	Wheel
$req$	Request
$max$	Maximum
$ele$	Electric
$ref$	Reference

## References

1. Ma, T.C.; Lin, W.K.; Yang, Y.B.; Wang, K.; Jia, W. Water content diagnosis for proton exchange membrane fuel cell based on wavelet transformation. *Int. J. Hydrogen Energy* **2020**, *45*, 20339–20350. [[CrossRef](#)]
2. Abaza, A.; Elsehiemy, R.A.; Mahmoud, K.; Lehtonen, M.; Darwish, M. Optimal Estimation of Proton Exchange Membrane Fuel Cells Parameter Based on Coyote Optimization Algorithm. *Appl. Sci.* **2021**, *11*, 2052. [[CrossRef](#)]
3. Al-Gabalawy, M.; Mahmoud, K.; Darwish, M.M.F.; Dawson, J.; Lehtonen, M.; Hosny, N. Reliable and Robust Observer for Simultaneously Estimating State-of-Charge and State-of-Health of LiFePO<sub>4</sub> Batteries. *Appl. Sci.* **2021**, *11*, 3609. [[CrossRef](#)]
4. Jahromi, M.M.; Heidary, H. Durability and economics investigations on triple stack configuration and its power management strategy for fuel cell vehicles. *Int. J. Hydrogen Energy* **2021**, *46*, 5740–5755. [[CrossRef](#)]
5. Ma, T.C.; Lin, W.K.; Yang, Y.B.; Cong, M.; Yu, Z.; Zhou, Q. Research on Control Algorithm of Proton Exchange Membrane Fuel Cell Cooling System. *Energies* **2019**, *12*, 3692. [[CrossRef](#)]
6. Xu, L.F.; Li, J.Q.; Hua, J.; Yang, G. Multi-mode control strategy for fuel cell electric vehicles regarding fuel economy and durability. *Int. J. Hydrogen Energy* **2014**, *39*, 2374–2389. [[CrossRef](#)]
7. Wang, Y.; Sun, Z.; Chen, Z. Rule-based energy management strategy of a lithium-ion battery, supercapacitor and PEM fuel cell system. *Energy Procedia* **2019**, *158*, 2555–2560. [[CrossRef](#)]
8. Ji, R.H. Optimal Design and Energy Management of Power System for Full-power Fuel Cell Vehicle. Master's Thesis, Jilin University, Changchun, China, 2020.
9. Wang, Y.G.; Suresh, D.A.; Ajay, K.P. A comparison of rule-based and model predictive controller-based power management strategies for fuel cell/battery hybrid vehicles considering degradation. *Int. J. Hydrogen Energy* **2020**, *45*, 33948–33956. [[CrossRef](#)]
10. Ahmadi, S.; Bathaee, S.M.T. Multi-objective genetic optimization of the fuel cell hybrid vehicle supervisory system: Fuzzy logic and operating mode control strategies. *Int. J. Hydrogen Energy* **2015**, *40*, 12512–12521. [[CrossRef](#)]
11. Wang, Y.J.; Sun, Z.D.; Chen, Z.H. Energy management strategy for battery/supercapacitor/fuel cell hybrid source vehicles based on finite state machine. *Appl. Energy* **2019**, *254*, 113707. [[CrossRef](#)]
12. Erdinc, O.; Vural, B.; Uzunoglu, M. A wavelet-fuzzy logic based energy management strategy for a fuel cell/battery/ultra-capacitor hybrid vehicular power system. *J. Power Sources* **2009**, *194*, 369–380. [[CrossRef](#)]
13. Fu, Z.; Zhu, L.; Si, P.; Sun, L. Optimization based energy management strategy for fuel cell/battery/ultracapacitor hybrid vehicle considering fuel economy and fuel cell lifespan. *Int. J. Hydrogen Energy* **2020**, *45*, 8875–8886. [[CrossRef](#)]
14. Ali, A.; Mahmoud, K.; Lehtonen, M. Multi-objective Photovoltaic Sizing with Diverse Inverter Control Schemes in Distribution Systems Hosting EVs. *IEEE Trans. Ind. Inform.* **2020**. [[CrossRef](#)]
15. Ferrario, A.M.; Manzano, F.S.; Bocci, E.; Andújar, J.M.; Bocci, E.; Martirano, L. Hydrogen vs. Battery in the Long-term Operation. A Comparative Between Energy Management Strategies for Hybrid Renewable Microgrids. *IEEE Consum. Electron. Mag.* **2020**, *9*, 1–128.
16. Koubaa, R.; Bacha, S.; Smaoui, M. Robust optimization based energy management of a fuel cell/ultra-capacitor hybrid electric vehicle under uncertainty. *Energy* **2020**, *200*, 117530. [[CrossRef](#)]
17. García, P.; Torreglosa, J.P.; Fernández, L.M.; Jurado, F. Control strategies for high-power electric vehicles powered by hydrogen fuel cell, battery and supercapacitor. *Expert Syst. Appl.* **2013**, *40*, 4791–4804. [[CrossRef](#)]
18. Geng, B.; Mills, J.K.; Sun, D. Two-Stage Energy Management Control of Fuel Cell Plug-In Hybrid Electric Vehicles Considering Fuel Cell Longevity. *IEEE Trans. Veh. Technol.* **2012**, *61*, 498–508. [[CrossRef](#)]
19. Xu, L.F.; Mueller, C.D.; Li, J.; Ouyang, M.; Hu, Z. Multi-objective component sizing based on optimal energy management strategy of fuel cell electric vehicles. *Appl. Energy* **2015**, *157*, 664–674. [[CrossRef](#)]
20. Hu, Z.Y.; Li, J.Q.; Xu, L.F.; Song, Z.; Fang, C.; Ouyang, M.; Dou, G.; Kou, G. Multi-objective energy management optimization and parameter sizing for proton exchange membrane hybrid fuel cell vehicles. *Energy Convers. Manag.* **2016**, *129*, 108–121. [[CrossRef](#)]
21. Zheng, C.H.; Kim, N.M.; Cha, S.W. Optimal control in the power management of fuel cell hybrid vehicles. *Int. J. Hydrogen Energy* **2012**, *37*, 655–663. [[CrossRef](#)]
22. Li, Q.; Chen, W.; Liu, Z.; Li, M.; Ma, L. Development of energy management system based on a power sharing strategy for a fuel cell-battery-supercapacitor hybrid tramway. *J. Power Sources* **2015**, *279*, 267–280. [[CrossRef](#)]
23. Florescu, A.; Bacha, S.; Munteanu, I.; Bratcu, A.I.; Rumeau, A. Adaptive frequency-separation-based Energy Management System for electric vehicles. *J. Power Sources* **2015**, *280*, 410–421. [[CrossRef](#)]
24. Li, T.; Liu, H.; Zhao, D.; Wang, L. Design and analysis of a fuel cell supercapacitor hybrid construction vehicle. *Int. J. Hydrogen Energy* **2016**, *41*, 12307–12319. [[CrossRef](#)]
25. Hou, Y.P.; Liu, Y.N.; Cai, Q.Z.; Sun, M. Study on efficiency characteristics of fuel cell engine during start-up. *Chin. J. Automot. Eng.* **2013**, *3*, 88–93.
26. Zhai, J.X.; He, G.L.; Xiong, Y.L. Experimental study on hydrogen utilization of proton exchange membrane fuel cell system. *Energy Storage Sci. Technol.* **2020**, *3*, 684–687.
27. Pei, P.C.; Chang, Q.; Tian, T. A quick evaluating method for automotive fuel cell lifetime. *Int. J. Hydrogen Energy* **2008**, *33*, 3829–3836. [[CrossRef](#)]
28. Jiang, H.L.; Xu, L.F.; Li, J.Q.; Hu, Z.; Ouyang, M. Energy Management and Component Sizing for a Fuel Cell/Battery/Supercapacitor Hybrid Powertrain based on Two-Dimensional Optimization Algorithms. *Energy* **2019**, *177*, 386–396. [[CrossRef](#)]

29. Liu, Y.G.; Liu, J.J.; Zhang, Y.J.; Wu, Y.; Chen, Z.; Ye, M. Rule learning based energy management strategy of fuel cell hybrid vehicles considering multi-objective optimization. *Energy* **2020**, *207*, 118212–118225. [[CrossRef](#)]
30. Song, K.; Chen, H.; Wen, P.M.; Zhang, T.; Zhang, B.; Zhang, T. A comprehensive evaluation framework to evaluate energy management strategies of fuel cell electric vehicles. *Electrochim. Acta* **2018**, *292*, 960–973. [[CrossRef](#)]
31. Shi, Y.Q.; He, B.; Cao, G.J.; Li, J.Q.; Ouyang, M.G. A study on the energy management strategy for fuel cell electric vehicle based on instantaneous optimization. *Automot. Eng.* **2008**, *1*, 30–35.
32. Shi, Y.Q.; He, B.; Cao, G.J.; Li, J.Q.; Ouyang, M.G. *Overview of NREL Battery Lifetime Models & Health Management R&D Health Management R&D for Electric Drive Vehicles*; National Renewable Energy Laboratory: Golden, CO, USA, 2012.
33. Li, F.; Yang, Z.P.; Wang, Y.; An, X.K.; Ling, F. Energy management strategy of tram with hybrid energy storage system based on pontryagin's minimum principle. *Trans. China Electrotech. Soc.* **2019**, *34*, 752–759.
34. Xu, L.F.; Ouyang, M.G.; Li, J.Q.; Yang, F.; Lu, L.; Hua, J. Application of Pontryagin's Minimal Principle to the energy management strategy of plugin fuel cell electric vehicles. *Int. J. Hydrogen Energy* **2013**, *38*, 10104–10115. [[CrossRef](#)]
35. Eudy, L. *Technology Acceleration: Fuel Cell Bus Evaluations*; National Renewable Energy Laboratory: Golden, CO, USA, 2019.
36. Wilson, A.; Kleen, G.; Papageorgopoulos, D. *Fuel Cell System Cost*; Department of Energy: Washington, DC, USA, 2017.
37. James, B.D. *2019 DOE Hydrogen and Fuel Cells Program Review Presentation*; Strategic Analysis Inc.: Reading, PA, USA, 2019.
38. AMPLY Power 2020. Unlocking the Cost-Saving Potential of Electric Fuel. Available online: <https://amplypower.com/whitepaper2020> (accessed on 31 May 2020).
39. Amwook, K.; Sukwon, C.; Huei, P. Optimal control of hybrid electric vehicles based on pontryagin's minimum principle. *IEEE Trans. Control Syst. Technol.* **2011**, *19*, 1279–1287.
40. Du, G.Q.; Xie, H.M.; Lu, Z.; Huang, Y. Analysis for the energy management problem of extended-range electric city buses based on pontryagin's minimum principle. *J. Chongqing Inst. Technol.* **2018**, *32*, 10–17.